CLASSIFICATION OF POLARIMETRIC SAR IMAGERY USING UNSUPERVISED H/α AND EXTENDED H/α SCHEMES TO DETECT ANOMALIES ON EARTHEN LEVEES

Ramakalavathi Marapareddy [1, 2], James V. Aanstoos[1], Nicolas H. Younan[2]

[1]*Geosystems Research Institute, Mississippi State University, MS 39759, USA*
[2]*Department of Electrical and Computer Engineering, Mississippi State University, MS 39762, USA*
Email: kala@gri.msstate.edu

ABSTRACT

Fully polarimetric Synthetic Aperture Radar (polSAR) data analysis has wide applications for terrain and ground cover classification. SAR technology, due to its high spatial resolution and soil penetration capability, is a good choice to identify problematic areas on earthen levees. In this paper, using the entropy (H), alpha angle (α), and eigenvalue parameters (λ), we implemented several unsupervised classification algorithms for the identification of anomalies on levees. The classification techniques applied here are: H/α classification and extended H/α (H/ α/λ) classification. In this work, the effectiveness of the algorithms was demonstrated using quad-polarimetric L-band SAR imagery from the NASA Jet Propulsion Laboratory's (JPL's) Uninhabited Aerial Vehicle Synthetic Aperture Radar (UAVSAR).

Keywords: Synthetic Aperture Radar, Earthen Levees, UAVSAR, Classification

1. INTRODUCTION

The dynamics of surface and subsurface water events on earthen levees can lead to slope instability resulting in slough slides. If these levees are not healthy, they may not be able to withstand flood conditions which could lead to catastrophic failures. Improved knowledge of the condition of these levees would significantly improve the allocation of precious resources to inspect, test, and repair the ones most in need [1]. Synthetic Aperture Radar (SAR) technology, due to its high spatial resolution and potential soil penetration capability, is a good choice to identify problematic areas on levees [1]. SAR polarimetry using quad-polarization data is the HV-polarization base in which an antenna transmits and receives horizontally and vertically polarized signals [2].

To facilitate the analysis of scattering mechanisms using eigen decomposition, three features are defined as a function of the eigenvalues and the eigenvectors of a spatial-power related 3x3 coherency matrix $\langle[T_3]\rangle$: (1) Entropy (H) which determines the randomness of scattering or degree of the statistical disorder of the target; (2) average alpha angle (α) for different scattering processes and identifying the dominant scattering mechanism; and (3) Lambda (λ) defined as nonnegative real eigenvalues of the diagonal matrix $[\Sigma_3]$ [3-4].

Cloude and Pottier [5] demonstrated an unsupervised classification based on the H/α parameters. These parameters alone were not sufficient for good interclass resolution, indicating that additional information is needed. Hellmann et. al. [6] tested an unsupervised classification based on the H/α/λ_1 parameters. However λ_1 alone was not able to represent the complete scattering mechanism about the target.

In this paper, we implemented several unsupervised classification algorithms for the identification of anomalies (slough slides) on the levee. The classification techniques applied are: H/α classification [5] and extended H/α (i.e., H/α/λ) classification [6-7], including classification for individual λ values as H/α/λ_1, H/α/λ_2, and H/α/λ_3. The work outlined here is focused on the H/α/λ (also using λ_1, λ_2, and λ_3) which takes advantage of individual classification using λ_1, λ_2, and λ_3 for a good interclass resolution. In this H/α/λ approach, the backscatter intensity information contained in the eigenvalues λ_1, λ_2, and λ_3 is used to improve the interclass resolution due to the different reflectivities of different scatterer.

2. METHODOLOGY

2.1 Polarimetric SAR Data Statistics

A polarimetric radar measures the complete scattering matrix [S] of a medium at a given incidence angle and for a given frequency [8]:

$$[S] = \begin{bmatrix} S_{HH} & S_{HV} \\ S_{HV} & S_{VV} \end{bmatrix} \quad (1)$$

This scattering matrix with complex elements can be expressed in a vector form, following:

$$\underline{X} = \begin{bmatrix} S_{HH} & \sqrt{2}S_{HV} & S_{VV} \end{bmatrix}^T \quad (2)$$

where the factor $\sqrt{2}$ arises from the requirement to keep the norm of the target vector $\underline{X}$ an invariant.
The target vector $\underline{k}$ is constructed from a linear combination of the elements of the scattering vector $\underline{X}$, following:

$$\underline{k} = \frac{1}{\sqrt{2}} \begin{bmatrix} S_{HH} + S_{VV} \\ S_{HH} - S_{VV} \\ 2S_{HV} \end{bmatrix} = \frac{1}{\sqrt{2}} \begin{bmatrix} 1 & 0 & 1 \\ 1 & 0 & -1 \\ 0 & 2 & 0 \end{bmatrix} \begin{bmatrix} S_{HH} \\ \sqrt{2}S_{HV} \\ S_{VV} \end{bmatrix} \quad (3)$$

The dimension of the target vector $\underline{k}$ is 3 due to the reciprocal case (S_{HV}=S_{VH}).

2.2 The H /α/λ Polarimetric Decomposition

The 3x3 coherency matrix [T] relates to the spatial-power. In the case of spatial-averaging, the expected value of the coherency matrix $\langle[T]\rangle$ is considered, representing the average distributed target as [3-5, 8]:

$$\langle[T]\rangle = \frac{1}{N}\sum_{i=1}^{N} \underline{k}_i . \underline{k}_i^{*T} = \frac{1}{N}\sum_{i=1}^{N}[T_i] \quad (4)$$

where the symbol *T stands for complex conjugate.
From this estimate, the eigenvectors and eigenvalues of the 3x3 coherency matrix $\langle[T]\rangle$ can be calculated to generate a diagonal form of the coherency matrix $\langle[T]\rangle$, which can be written in the form:

$$\langle[T_3]\rangle = [U_3][\Sigma][U_3]^{-1} \quad (5)$$

where $[\Sigma]$ is a 3x3 diagonal matrix with nonnegative real elements (eigenvalues) of $\langle[T_3]\rangle$ and $[U_3] = [\underline{u}_1 \quad \underline{u}_2 \quad \underline{u}_3]$ is a 3x3 unitary matrix, where $\underline{u}_1$, $\underline{u}_2$, and $\underline{u}_3$ are the three unit orthogonal eigenvectors of $\langle[T_3]\rangle$, and:

$$[\Sigma_3] = \begin{bmatrix} \lambda_1 & 0 & 0 \\ 0 & \lambda_2 & 0 \\ 0 & 0 & \lambda_3 \end{bmatrix} \quad (6)$$

where $\lambda_1 > \lambda_2 > \lambda_3 > 0$.

The polarimetric parameterization of the unit target vector $\underline{u}$ involves the combination of three simple scattering mechanisms: surface scattering, double-bounce scattering, and volume scattering, in the case of a distributed target (natural media), which are characterized from the three components (target generators) of the unit target vector [3, 9]. For the mono-static case, the 3x3 coherency matrix $[T]$ has the following parameterization [3]:

$$[T] = \underline{k}.\underline{k}^{*T} = \begin{bmatrix} 2A_0 & C - jD & H + jG \\ C + jD & B_0 + B & E + jF \\ H - jG & E - jF & B_0 - B \end{bmatrix} \quad (7)$$

Surface Scattering: $A_0 \gg B_0 + B,\ B_0 - B$
Double-bounce Scattering: $B_0 + B \gg A_0,\ B_0 - B$
Volume Scattering: $B_0 - B \gg A_0,\ B_0 + B$

It is possible to use these target generators to create a color coding for PolSAR images, by assigning different the colors [9]:

Blue for Surface Scattering: $2A_0 = |S_{HH} + S_{VV}|$
Red for double-bounce Scattering: $B_0 + B = |S_{HH} - S_{VV}|$
Green for Volume Scattering: $B_0 - B = |S_{HV}|$

2.3. Classification based on H /α/λ Polarimetric Decomposition

Cloude and Pottier's [3] decomposition based on the eigenvalue analysis of a coherency matrix,$\langle[T]\rangle$ is:

$$\langle[T]\rangle = \lambda_1 u_1 e_1^{*T} + \lambda_2 u_2 e_2^{*T} + \lambda_3 u_3 e_3^{*T} \quad (8)$$

where λ_i and u_i for $i = 1, 2, 3$ are eigenvalues and eigenvectors. The eigenvectors can be written as

$$\underline{u}_i = [\cos\alpha_i \quad \sin\alpha_i \cos\beta_i e^{j\delta_i} \quad \sin\alpha_i \cos\beta_i e^{j\gamma_i}]^T \quad (9)$$

Cloude and Pottier defined three parameters as a function of the eigenvalues and the eigenvectors of$\langle[T_3]\rangle$ [3-5, 9]:

Entropy (H): determines the degree of statistical disorder of each target.

$$H = -\sum_{i=1}^{3} P_i \log_3(P_i) \quad (10)$$

$$P_i = \frac{\lambda_i}{\sum_{j=1}^{3}\lambda_j} \quad (11)$$

where P_i is the probability of the eigenvalue λ_i.

The entropy, ranging from 0 to 1, represents the randomness of a scattering medium from isotropic scattering (H=0) to totally random scattering (H=1). For ocean and less rough surfaces, surface scattering will dominate, and H is near 0. For heavily vegetated areas, the H value will be high, due to multiple scattering mechanisms.
Span (λ): represents the total scattered power.

$$span = |S_{HH}|^2 + |S_{VV}|^2 + 2|S_{HV}|^2 = \sum_{i=1}^{3}\lambda_i \quad (12)$$

$$span = Trace\,([\Sigma_3]) = \sum_{i=1}^{3}\lambda_i \quad (13)$$

$$\lambda = \sum_{i=1}^{3}\lambda_i = \lambda_1 + \lambda_2 + \lambda_3 \quad (14)$$

Average alpha angle (α): identifies the dominant scattering mechanism for different scattering processes.

$$\alpha = \sum_{i=1}^{3} P_i\alpha_i = P_1\alpha_1 + P_2\alpha_2 + P_3\alpha_3 \quad (15)$$

α reveals the averaged scattering mechanisms from surface scattering (α =0) to double bounce scattering (α=90).

For classification, the H and α plane is divided into nine zones [5], as shown in Fig. 1. The region outside the curve including Z3 represents mathematically infeasible combinations of H and α values. Pixels within each of the other zones are considered to belong to a class associated with that zone. The classification approach presented in this paper uses the H/α features, enhanced by the use of the eigenvalues of the eigenvalue analysis of a coherency matrix, $\langle[T]\rangle$.The physical scattering characteristics of each of the zones are as follows [5]: Z9: Low Entropy Surface Scattering; Z8: Low Entropy Dipole Scattering; Z7: Low Entropy Multiple Scattering; Z6: Medium Entropy Surface Scattering; Z5: Medium Entropy Vegetation Scattering; Z4: Medium Entropy Multiple Scattering; Z3: (Not a Feasible Region); Z2: High Entropy Vegetation Scattering; and Z1: High Entropy Multiple Scattering.

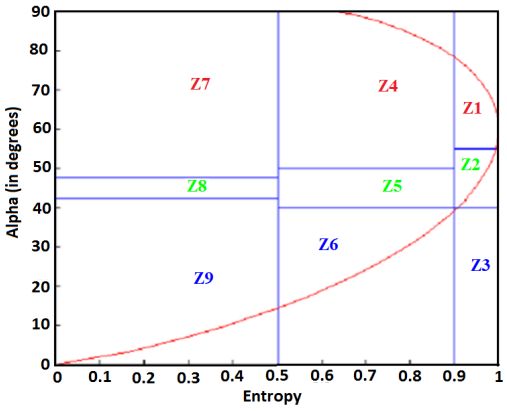

Fig. 1. H/α plane for random media scattering [8].

3. DATA AND STUDY AREA USED

The fully quad-polarimetric L-band (λ = 23.98 cm) SAR imagery from the NASA Jet Propulsion Laboratory's (JPL's) Uninhabited Aerial Vehicle Synthetic Aperture Radar (UAVSAR) with a range bandwidth of 80 MHz (resulting ~ 1 m range resolution) was used to detect anomalies on earthen levees. A multi-polarized UAVSAR image acquired on June 16, 2009 is used for this work. The HHVV MLC (multi-look cross product) data was chosen for the classification, because the phase difference

between the HH and VV polarized backscatter contains a good range of information for natural targets [10]. We also relied on the ground truth data collected by the US Army Corps of Engineers (USACE) which documented the location and timing of slough slide appearance and repair history. The ground truth data was also compared to the optical NAIP (National Agriculture Imagery Program) data to visually confirm the slide events. The proposed algorithms were applied to a subset area of levee. The study area, as shown in Figure 2, is a section of the lower the Mississippi River valley in the southern USA, where earthen flood control levees are maintained by the US Army Corps of Engineers.

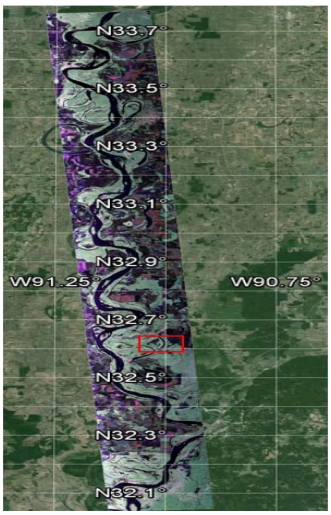

Fig. 2. Study area with radar color composite and subset area marked with red box.

4. RESULTS AND DISCUSSION

The PolSAR data was used for classification of scattering mechanisms of a target having a particular scattering process, such as surface, double-bounce, or volume scattering [9]. Figures 3 (a-c) show the images of Eigen decomposition parameters such as entropy, alpha, and lambda. Figures 4 (a-f) show the images of: (a) Pauli RGB image with subset area marked with a red rectangle, (b) H/α classification, (c) H/α/λ classification, (d) H/α/λ_1 classification, (e) H/α/λ_2 classification, and (f) H/α/λ_3 classification. The slough slide locations are marked as polygon on the images and testing area (river side of the levee) is marked with shape area on the images. H/α classification is classified into 9 classes based on the H/α segmentation plane [5] as shown in the Fig. 4(b). Whereas, H/α/λ, H/α/λ_1, H/α/λ_2, and H/α/λ_3 classifications are inter-classified within the 9 classes as shown in the Figures 4 (c-f) to represent the interclass resolution due to the different reflectivities of different scatterers [6-7].

All the segmentation class values of segmented zones for the H/α, H/α/λ_1, H/α/λ_2, and H/α/λ_3 classifications using the H/α segmentation plane for random media scattering are listed in the Table 1. Using these values the classification color map representing each class of H/α/λ classification is extended to 27 colors from 9. In the classification with individual eigenvalues analysis, the H/α/λ_1 classification shows where surface scattering dominates; the H/α/λ_2 classification highlights areas dominated by double-bounce scattering; and in the H/α/λ_3 classification the volume scattering is emphasized. For the slough slide areas, it can be seen that the surface scattering is partially dominant, the double-bounce scattering is strongly dominant, and the volume scattering is almost zero, since here our target (levee) is the naturally distributed. The Polarimetric SAR data processing and educational tool (PolSARpro v4.2.0 software) from the European Space Agency was used for this work [11].

Table 1. Class values of segmented zones for the H/α, H/α/λ_1, H/α/λ_2, and H/α/λ_3 classifications using the H/α segmentation plane for random media scattering

Zone\Class value	Classification			
	H/α	H/α/λ_1	H/α/λ_2	H/α/λ_3
Z1	1	1	3.37	6.54
Z2	2	1.31	4.08	6.85
Z3	0	0	0	0
Z4	4	1.92	4.69	8.38
Z5	5	2.23	5.00	7.77
Z6	6	2.54	5.31	8.08
Z7	7	2.85	5.62	8.38
Z8	8	3.15	5.92	8.69
Z9	9	3.46	6.23	0

5. CONCLUSION AND FUTURE WORK

The H/α classification and H/α/λ (also individually including λ_1, λ_2, and λ_3) classification were applied to polarimetric data. This work shows that slough slides on levees exhibit distinctive scattering mechanisms compared with the healthy (i.e., non-slough slide) areas, and that these differences are revealed by unsupervised classification methods utilizing the polarimetric decomposition parameters H, α, and λ. Hence, the resulting color coded class maps can be used to detect anomalous areas on the levee for closer inspection. The obtained classification results reveal that the H/α/λ classification method provides superior classification compared to the other unsupervised classification schemes for this application. The efficacy of the algorithms was demonstrated using quad-polarimetric L-band UAVSAR data. In future work to improve the classification accuracy of anomaly detection on levees, we plan to test statistics-based classifiers which incorporate these features and thus benefit from their explicit representation of dominant polarimetric scattering mechanisms.

ACKNOWLEDGEMENT

This material is based upon work supported by the National Science Foundation under Award No. OISE-1243539, and by the NASA Applied Sciences Division under grant number NNX09AV25G. The authors would like to thank the US Army Corps of Engineers, Engineer Research and Development Center and Vicksburg Levee District for providing ground truth data and expertise; and also NASA Jet Propulsion Laboratory's for providing the UAVSAR images.

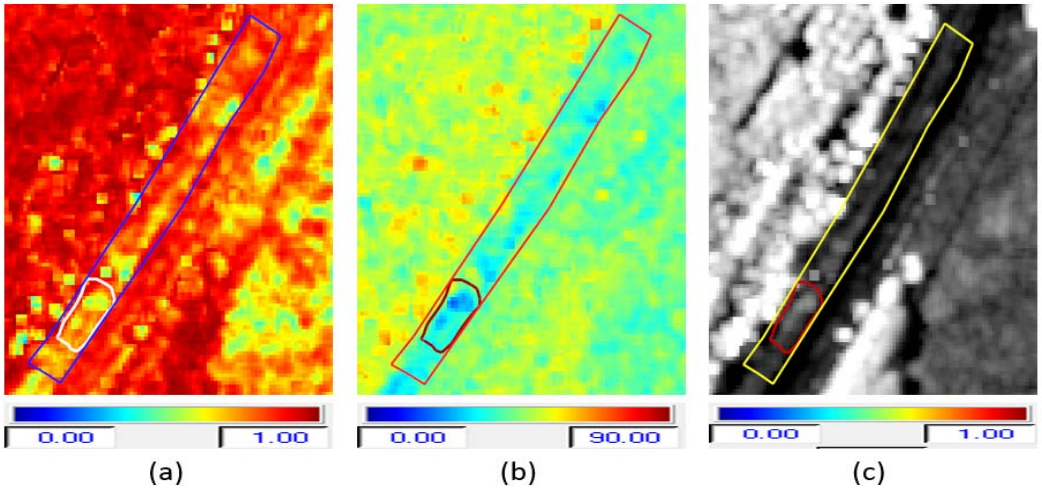

Figure 3 (a-c). Entropy, alpha, and lambda.

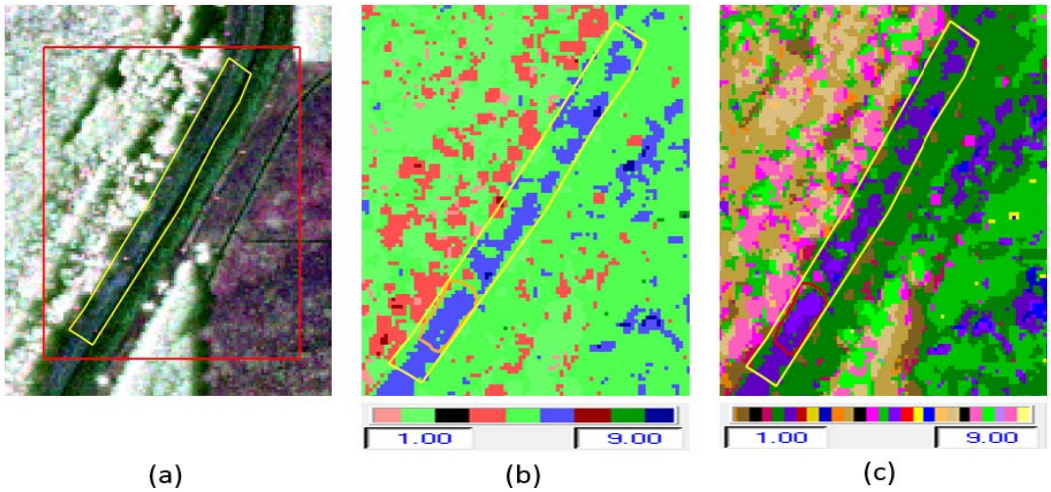

Figure 4(a-c). Pauli RGB Image, H/α classification, and H/α/λ classification.

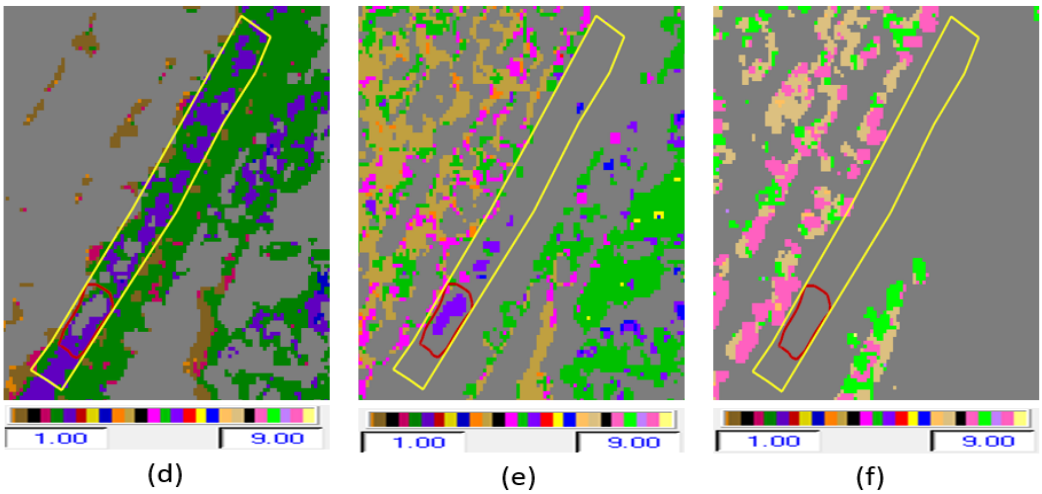

Figure 4(d-f). H/α/λ_1, H/α/λ_2, and H/α/λ_3 classification.

REFERENCES

[1] J.V. Aanstoos, K. Hasan, C. O\'Hara, L. Dabbiru, M. Mahrooghy, R. A. A. Nobrega, and M. Lee, "Detection of Slump Slides on Earthen Levees Using Polarimetric SAR Imagery," *IEEE Applied Imagery Pattern Recognition Workshop,* 2012.

[2] K. Ouchi, "Recent Trend and Advance of Synthetic Aperture Radar with Selected Topics," *Remote Sens.*, vol.5, no. 2, pp. 716-807, 2013.

[3] S.R. Cloude and E. Pottier, "A review of target decomposition theorems in radar polarimetry," *IEEE Trans. Geosci. Remote Sens.*, vol.34, no.2, pp. 498–518, 1996.

[4] T.L. Ainsworth, S.R. Cloude, and J.S. Lee, "Eigenvector analysis of polarimetric SAR data," *IEEE International Geosci. Remote Sens. Symposium*, vol.1, pp. 626-628, 2002.

[5] S.R. Cloude and E. Pottier, "An entropy based classification scheme for land applications of polarimetric SAR," *IEEE Trans. Geosci. Remote Sens.*, vol.*35*, no.1, pp. 68–78, 1997.

[6] M. Hellmann, G. Jager, E. Kratzschmar, and M. Habermeyer, "Classification of full polarimetric SAR-data using artificial neural networks and fuzzy algorithms," *Geosci. Remote Sens. Symposium*, *IEEE International*, vol.4, pp.1995-1997, 1999.

[7] M. Hellmann, G. Jager, and E. Pottier, "Fuzzy clustering and interpretation of fully polarimetric SAR data," *Geosci. Remote Sens. Symposium, IEEE International*, vol.6, pp. 2790-2792, 2001.

[8] J.S. Lee, M.R. Grunes, T.L. Anisoworth, L.J. Du, D. L. Schuler, S.R. Coulde, "Unsupervised classification using polarimetric decomposition and the complex Whishart classifier," *IEEE Trans. Geosci. Remote Sens.,* vol.*35*, no.5, pp. 2249–2258, 1999.

[9] A. Freeman and S.T. Durden, "A Three-Component Scattering Model for Polarimetric SAR Data," *IEEE Trans. Geosci. Remote Sens.*, vol. 36, no. 3, pp. 963-973, 1998.

[10] Y. Oh and G. Chang, "Classification of Polarimetric SAR Images using the Degree of polarization and the Co-Polarized Phase Difference," *Geosci. Remote Sens. Symposium, IEEE International*, vol.5, pp. 362-365, 2008.

[11] PolSARpro (Polarimetric SAR Data Processing and Educational Tool v4.0) Software, https://earth.esa.int/web/polsarpro/download/release-notes/previous-versions/-/article/version-4-1-5-to-version-4-2.